Received: 6 February 2020 | Revised: 6 March 2020 | Accepted: 13 March 2020

DOI: 10.1002/qua.26228



FULL PAPER

International Journal of Quantum Chemistry WILEY

# Frozen-density embedding-based many-body expansions

Daniel Schmitt-Monreal | Christoph R. Jacob

Institute of Physical and Theoretical Chemistry, Technische Universität Braunschweig, Braunschweig, Germany

**Correspondence**
Christoph R. Jacob, Institute of Physical and Theoretical Chemistry, Technische Universität Braunschweig, Gaußstraße 17, 38106 Braunschweig, Germany.
Email: c.jacob@tu-braunschweig.de

## Abstract

Fragmentation methods allow for the accurate quantum chemical (QC) treatment of large molecular clusters and materials. Here we explore the combination of two complementary approaches to the development of such fragmentation methods: the many-body expansion (MBE) on the one hand, and subsystem density-functional theory (DFT) or frozen-density embedding (FDE) theory on the other hand. First, we assess potential benefits of using FDE to account for the environment in the subsystem calculations performed within the MBE. Second, we use subsystem DFT to derive a density-based MBE, in which a many-body expansion of the electron density is used to calculate the system's total energy. This provides a correction to the energies calculated with a conventional energy-based MBE that depends only on the subsystem's electron densities. For the test case of clusters of water and of aspirin, we show that such a density-based MBE converges faster than the conventional energy-based MBE. For our test cases, truncation errors in the interaction energies are below chemical accuracy already with a two-body expansion. The density-based MBE thus provides a promising avenue for accurate QC calculation of molecular clusters and materials.

**KEYWORDS**

frozen-density embedding, many-body expansion, molecular clusters, quantum embedding

## 1 | INTRODUCTION

The development of fragmentation methods for quantum chemistry in the past decades has enabled researchers to tackle chemical systems of increasing complexity with accurate computational methods.[1–4] By partitioning a large molecular or bulk-phase system into smaller subsystems, fragmentation methods allow for an efficient, yet accurate quantum chemical (QC) treatment. On the one hand, fragmentation methods make it possible to focus on one or a few subsystems of interest (eg, a reaction center or a chromophore), which are embedded in a complex environment.[5,6] Numerous embedding strategies have been developed to account for environmental effects on the subsystems of interest, ranging from continuum solvation models[7,8] and classical QM/MM (quantum mechanical/molecular mechanics) embedding schemes[9–11] to quantum embedding methods.[12–16] The latter maintain a QM description of the environment, which enters the QC calculation of the subsystems of interest either via its electron density[12–14] or via its one-electron orbitals.[15,16] Quantum embedding methods have, for instance, been employed for the prediction of local spectroscopic properties in solution[17–19] and in biomolecular environments,[20–22] for the computation of reaction energetics in enzymes,[23,24] and for modeling of quantum dynamics in scattering experiments.[25]

On the other hand, fragmentation methods can be used to efficiently obtain properties of large chemical systems in which all subsystems need to be treated on an equal footing.[26–29] An important and still challenging example is the prediction of energy differences between

conformers of large molecular clusters or between different polymorphs of molecular crystals.[30] Here, a balanced treatment of different types of intermolecular interactions (eg, hydrogen bonding, $\pi$-$\pi$ stacking, C—H $\cdots\pi$ interactions, dipole-dipole interaction, dispersion interactions) is required, which demands the use of high-level QC methods.[31,32] However, such methods show a steep scaling of the computational cost with system size, which precludes their direct application to larger clusters or bulk-phase systems. Then again, molecular clusters and crystals can be naturally partitioned into molecular subsystems and thus appear to be ideally suited for fragmentation methods.

A straightforward and conceptually simple fragmentation approach to molecular clusters and crystals is provided by the many-body expansion (MBE),[33–40] in which QC calculations of subsystems of increasing size (ie, monomers, dimers, trimers, etc.) are used to expand the system's total energy as

$$E_{\text{tot}} = \sum_I E_I^{(1)} + \sum_{I<J} \Delta E_{IJ}^{(2)} + \sum_{I<J<K} \Delta E_{IJK}^{(3)} + \cdots \tag{1}$$

Here, $E_I^{(1)} = E_I$ is the energy of the $I$th monomer. The interaction energy $\Delta E_{IJ}^{(2)}$ of the dimer consisting of monomers $I$ and $J$ is calculated as

$$\Delta E_{IJ}^{(2)} = E_{IJ} - E_I - E_J, \tag{2}$$

and that of the trimer interaction is obtained as

$$\Delta E_{IJK}^{(3)} = E_{IJK} - \Delta E_{IJ}^{(2)} - \Delta E_{IK}^{(2)} - \Delta E_{JK}^{(2)} - E_I - E_J - E_K. \tag{3}$$

Higher order interaction energies are defined analogously (see Refs. [37, 41]). Such an MBE can be applied in combination with any QC method, and the individual QC calculations can easily be performed in an embarrassingly parallel fashion (see, eg, Refs. [42, 43]).

While it is ensured that the MBE converges to the exact total energy of the full supermolecular system, the number of $n$-mers increases rapidly at higher orders. Therefore, in practice the MBE is useful only if it can be truncated at low order, and strategies of accelerating the convergence of the MBE are necessary if one seeks to treat larger molecular clusters or molecular crystals accurately with high-level QC methods.

To this end, two complementary strategies are commonly pursued (see Herbert[40] for a comprehensive review). First, the MBE can be combined with embedding methods for the individual subsystem calculations.[44–46] By accounting for the effect of the environment on the subsystems, this makes it possible to partly include higher order many-body effects in the low-order contributions. So far, classical embedding schemes are widely used within the MBE, for example, by using point charges extracted from monomer calculations or by using partial-charge parametrizations from suitable force fields.[47] While quantum embedding schemes have been shown to be able to account for environment effects on local molecular properties more accurately than classical embedding methods,[5,48,49] their use within the MBE remains mostly unexplored. Exceptions are the use of the XPol approach in the variational many-body method[50] as well as different variants of the fragment-molecular orbital method.[51–53] Recently, Head-Gordon and coworkers[54] have assessed the use of a quantum embedding scheme within MBE by applying the embedded mean-field theory of Manby and Miller[55] for the subsystem calculations.

Second, cheap low-level computational methods can be applied to calculate the higher order contributions which are otherwise neglected in a truncated MBE, following the idea of the ONIOM approach.[56–58] This can be used to construct multilevel composite methods based on the MBE.[59,60] The hybrid many-body interactions method of Beran and coworkers,[61,62] which has been successfully applied to calculate the energy differences between polymorphs of molecular crystals, uses a MBE up to two-body contributions in combination with a classical polarizable force field to account for many-body polarization effects. While such ONIOM-type composite approaches are in principle complementary to the use of an embedded MBE, it is often unclear how to avoid double counting when combining these two strategies.

Here, we apply quantum embedding within both of these strategies for accelerating the convergence of the MBE for molecular clusters. Specifically, as a quantum embedding approach we use frozen-density embedding (FDE) theory,[14,63] which provides a formally exact subsystem density functional theory (DFT) method.[12] In FDE, the embedding potential and the interaction energies between subsystems depend only on the subsystems' electron densities, which makes it possible to incorporate arbitrary QC methods into the FDE framework.[64–66] First, we explore the possible advantages of using FDE as an embedding method for the subsystem calculations within the MBE. Second, we propose a density-based MBE that makes use of the framework of FDE by starting from a MBE of the electron density. This provides an interaction energy correction that accurately accounts for higher-order energy contributions, which are neglected in a conventional truncated MBE.

The rest of the paper is organized as follows. In Sections 2.1 and 2.2 we review the conventional energy-based MBE as well as different embedding schemes that can be applied for the subsystem calculations. For the test case of water clusters, in Section 2.3 we then assess the convergence of the truncated MBE performed using isolated as well as embedded subsystems. In Section 2.4, the many-body convergence of the electron density is analyzed. In Section 3.1, we present the theory of our density-based MBE, which is subsequently tested and analyzed for water clusters (Section 3.2) and for clusters of aspirin (Section 3.2). Finally, a summary and conclusions are presented in Section 4. Details of our implementation and computations are given at the end of the article.

## 2 | ENERGY-BASED MANY-BODY EXPANSION

### 2.1 | Isolated many-body expansion

The many-body expansion decomposes the total energy of a system consisting of $N$ molecular fragments into one-body, two-body, three-body, etc. contributions (cf. Equation (1)):

$$E_{\text{tot}} = E^{(1)} + \Delta E^{(2)} + \Delta E^{(3)} + \cdots = E^{(1)} + \sum_{i=2}^{N} \Delta E^{(i)}, \tag{4}$$

with the one-body contribution $E^{(1)} = \sum_I E_I^{(1)}$, the two-body contribution $\Delta E^{(2)} = \sum_{I<J} \Delta E_{IJ}^{(2)}$, the three-body contribution $\Delta E^{(3)} = \sum_{I<J<K} \Delta E_{IJK}^{(3)}$, and so on.[37,40] These $n$-body contributions are obtained from calculations for subsystems consisting of up to $n$ molecular fragments. By construction, this many-body decomposition of the total energy is exact if all terms up to order $N$ are included.

The above expression corresponds to an *energy-based* many-body expansion (eb-MBE), that is, it considers only the total energies obtained from the calculations of the monomer, dimer, trimer, etc. subsystems. Conventionally, these are obtained from QC calculations that consider the isolated subsystems (ie, the remaining molecular fragments are completely ignored). We will refer to this type of many-body expansion as *isolated* energy-based MBE.

Within DFT,[67,68] the total energy of the subsystem consisting of molecular fragments {$I$, $J$, ...} is calculated as

$$E_{IJ\ldots}[\rho_{IJ\ldots}] = T_s[\rho_{IJ\ldots}] + V_{\text{nuc}}^{(IJ\ldots)}[\rho_{IJ\ldots}] + J[\rho_{IJ\ldots}] + E_{\text{xc}}[\rho_{IJ\ldots}] + E_{\text{NN}}^{(IJ\ldots)}, \tag{5}$$

where $\rho_{IJ\ldots}$ denotes the electron density of the subsystem consisting of molecular fragments {$I$, $J$, ...}. Here, the nuclei-electron attraction energy can be decomposed into contributions due to the nuclei of each of the molecular fragments, $V_{\text{nuc}}^{(IJ\ldots)}[\rho_{IJ\ldots}] = \sum_{K\in\{I,J,\ldots\}} V_{\text{nuc}}^{(K)}[\rho_{IJ\ldots}]$, where

$$V_{\text{nuc}}^{(K)}[\rho_{IJ\ldots}] = \int \rho_{IJ\ldots}(\boldsymbol{r}) v_{\text{nuc}}^{(K)}(\boldsymbol{r}) \mathrm{d}^3 r \quad \text{with} \quad v_{\text{nuc}}^{(K)}(\boldsymbol{r}) = \sum_{i\in K} \frac{Z_i}{|\boldsymbol{r} - \boldsymbol{R}_i|}. \tag{6}$$

and the nuclear repulsion energy can be decomposed into contributions of pairs of molecular fragments, $E_{\text{NN}}^{(IJ\ldots)} = \frac{1}{2}\sum_{K,L\in\{I,J,\ldots\}} E_{\text{NN}}^{(KL)}$ with

$$E_{\text{NN}}^{(KL)} = \sum_{k\in K}\sum_{\substack{l\in L \\ l\neq k}} \frac{Z_k Z_l}{|\boldsymbol{R}_k - \boldsymbol{R}_l|}. \tag{7}$$

The electronic Coulomb repulsion energy is given by

$$J[\rho_{IJ\ldots}] = \frac{1}{2}\int\int \frac{\rho_{IJ\ldots}(\boldsymbol{r})\rho_{IJ\ldots}(\boldsymbol{r}')}{|\boldsymbol{r} - \boldsymbol{r}'|} \mathrm{d}^3 r \mathrm{d}^3 r'. \tag{8}$$

Finally, the noninteracting kinetic energy $T_s[\rho_{IJ\ldots}]$ is evaluated from the Kohn-Sham (KS) orbitals $\{\phi_i\}$ of the KS reference system with electron density $\rho_{IJ\ldots}$, and the exchange-correlation (xc) energy $E_{\text{xc}}[\rho_{IJ\ldots}]$ is commonly evaluated using an approximate xc functional.

In the isolated eb-MBE case, the subsystem densities $\rho_{IJ\ldots}$ are obtained by minimizing the total energy functional of Equation (5), which leads to the well-known KS equations for the subsystem's KS orbitals. No additional terms due to the remaining molecular fragments are included in these KS equations.

While in the following we will mostly use the conceptual framework of DFT, the subsystem energies can also be obtained with wavefunction-based QC methods.[64–66] In this case, the total energy of the isolated subsystem consisting of molecular fragments {$I$, $J$, ...} is calculated as

$$E_{IJ\ldots} = \left\langle \Psi_{IJ\ldots} | \hat{H}^{(IJ\ldots)} | \Psi_{IJ\ldots} \right\rangle, \tag{9}$$

and the wavefunction $\Psi_{IJ\ldots}$ is obtained as an (approximate) eigenfunction of the subsystem's Hamiltonian $\hat{H}^{(IJ\ldots)} = \hat{T} + \hat{V}_{\text{nuc}}^{(IJ\ldots)} + \hat{V}_{ee} + E_{\text{NN}}^{(IJ\ldots)}$. Again, in the case of the isolated eb-MBE, no additional terms due to the remaining molecular fragments are included in this Hamiltonian.

In the energy-based many-body expansion, $N$ QC calculations for monomers are required to obtain the one-body contributions, $N(N-1)/2$ calculations for dimers to obtain the two-body contributions, and $\binom{N}{n}$ calculations for $n$-mers to obtain the $n$-body contributions. A computational advantage compared to the calculation for the full system can be exploited only if the many-body expansion is truncated at a sufficiently low order $n \ll N$, that is

$$E_{\text{tot}} \approx E_{\text{eb}}^{(n)} = E^{(1)} + \sum_{i=2}^{n} \Delta E^{(i)}. \tag{10}$$

Thus, whether the MBE is useful as a tool for the QC treatment of large molecular clusters and crystals is dependent on the fast convergence of the MBE.

## 2.2 | Embedded many-body expansion

A commonly used strategy for accelerating the convergence of the eb-MBE is to approximately include the environment into the QC calculations performed for the subsystems.[44–47] For the subsystem composed of the molecular fragments {*I*, *J*, …}, the effect of this environment is included as a (local) embedding potential, $v_{\text{emb}}^{(IJ\ldots)}(\boldsymbol{r})$, which is due to the remaining molecular fragments $K \notin \{I, J, \ldots\}$.

Within the framework of DFT, this embedding potential is included in the KS equations for the considered subsystem, whereas within wavefunction-based calculations it is included via an embedding operator $\hat{V}_{\text{emb}}^{\{IJ\ldots\}} = \sum_i v_{\text{emb}}^{(IJ\ldots)}(\boldsymbol{r}_i)$. Thus, it will change the subsystem's electron density $\rho_{IJ\ldots}$ or its wavefunction $\Psi_{IJ\ldots}$, which is subsequently used to evaluate the subsystem's energy according to Equation (5) or (9), respectively. Note that no explicit embedding energy contributions enter the eb-MBE: that is, there are no contributions of the embedding potential in Equations (5) and (9). Consequently, only energy terms that refer to the embedded subsystems are included in the expansion of Equation (1). This is necessary to prevent double counting of such contributions in eb-MBE. Note that for technical reasons, in some implementations, embedding energy contributions are included in the subsystem energies but they are subsequently removed via a suitable self-energy correction.[69,70]

A widely used example for such an *embedded* eb-MBE is the electrostatically embedded many-body expansion (EE-MBE),[44,45] which uses the embedding potential

$$v_{\text{emb,PC}}^{(IJ\ldots)}(\boldsymbol{r}) = \sum_{K \notin \{I,J,\ldots\}} \sum_{k \in K} \frac{q_k}{|\boldsymbol{r} - \boldsymbol{R}_k|} \tag{11}$$

where $q_k$ are suitable partial charges placed at the positions of the nuclei $\boldsymbol{R}_k$. Such an electrostatic point-charge embedding (PCE) is commonly used in the context of QM/MM methods. It has been previously shown that it can accelerate the convergence of the eb-MBE for molecular clusters compared to the isolated eb-MBE.[44,45,71,72]

As an alternative to an electrostatic PCE, we also consider the embedding potential of FDE theory[12,14,63]:

$$\begin{aligned} v_{\text{emb,FDE}}^{(IJ\ldots)}(\boldsymbol{r}) \;=\; & \sum_{K \notin \{I,J,\ldots\}} v_{\text{nuc}}^{(K)}(\boldsymbol{r}) + \sum_{K \notin \{I,J,\ldots\}} \int \frac{\rho_K(\boldsymbol{r}')}{|\boldsymbol{r} - \boldsymbol{r}'|} \mathrm{d}^3 r' \\ & + \frac{\delta T_s[\rho]}{\delta \rho}\bigg|_{\rho = \rho_{\text{tot}}} - \frac{\delta T_s[\rho]}{\delta \rho}\bigg|_{\rho = \rho_{IJ\ldots}} + \frac{\delta E_{\text{xc}}[\rho]}{\delta \rho}\bigg|_{\rho = \rho_{\text{tot}}} - \frac{\delta E_{\text{xc}}[\rho]}{\delta \rho}\bigg|_{\rho = \rho_{IJ\ldots}} \end{aligned} \tag{12}$$

with $\rho_{\text{tot}} = \rho_{IJ\ldots} + \sum_{K \notin \{I,J,\ldots\}} \rho_K$. This embedding potential contains the full electrostatic interaction as well as nonclassical contributions due to the xc and kinetic energy. It is formally exact in the sense that, with the exact functionals and suitable environment electron densities, it will lead to the exact total density.[73,74] However, in practice an approximate local xc functional and an approximate nonadditive kinetic energy functional have to be used.[12,75,76]

Compared to the electrostatic PCE potential, the FDE potential does not rely on the parameterization of point charges. Furthermore, by fully accounting for the electrostatic and nonclassical interactions it should be possible to describe the effect of the environment on the considered active subsystem more accurately. It has previously been shown that for the calculation of spectroscopic properties, FDE is usually superior to a simple PCE as used in conventional QM/MM methods.[5,48,49,66] Here, we want to explore possible advantages of the FDE potential within the eb-MBE. The different variants of the MBE that are studied in this work are summarized in Table 1.

**TABLE 1** Overview of the different variants of the many-body expansion (MBE) and embedding schemes that are studied in this work, along with the corresponding acronyms used in the figures and tables

| MBE variant | Acronym | Definition |
|---|---|---|
| Energy-based | eb-MBE | Equation (10) |
| Density-based | db-MBE | Equation (22) |
| **Embedding scheme** | **Acronym** | $v_{\text{emb}}^{(IJ\cdots)}(\mathbf{r})$ |
| Isolated | iso | — |
| Point charges | PC | Equation (11) |
| Frozen density | FDE | Equation (12) |

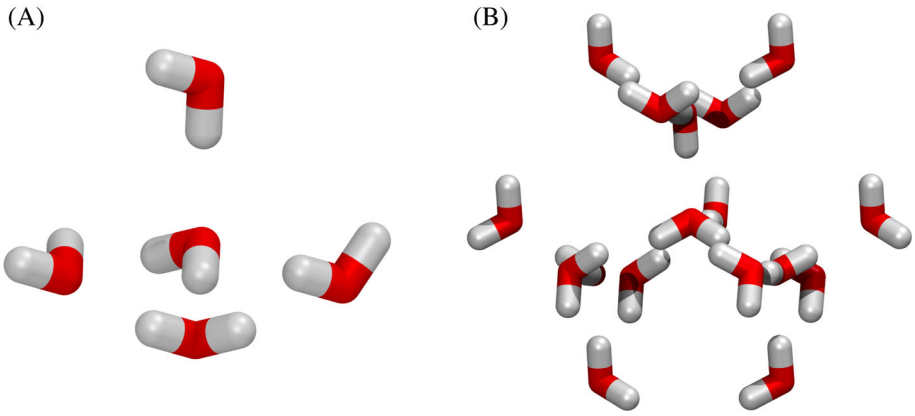


**FIGURE 1** Structure of the water clusters considered as a test case; A, $(H_2O)_5$ and B, $(H_2O)_{17}$. The structures of these clusters have been extracted from the crystal structure of ice $I_h$

## 2.3 | Test case: Water clusters

Water clusters present a challenging test case for the MBE because of the large many-body polarization effects that need to be captured.[38,44,72,77–80] Here, we consider water clusters extracted from the crystal structure of ice $I_h$.[81,82] First, we use a water pentamer, $(H_2O)_5$, in which the central water molecule is surrounded by four water molecules in a pseudo-tetrahedral environment (see Figure 1A). Second, we consider an $(H_2O)_{17}$ cluster, in which a second shell of water molecules has been added to the pentamer, that is, each of the surrounding water molecules in the pentamer is now coordinated to three additional water molecules that complete its pseudo-tetrahedral environment (see Figure 1B).

We aim at calculating the interaction energy *per molecule* between the water molecules in these clusters, that is

$$E_{\text{int}} = \frac{1}{N}\left(E_{\text{tot}} - \sum_I E_I^{(1)}\right) = \frac{1}{N}\left(E_{\text{tot}} - E_{\text{eb,iso}}^{(1)}\right). \tag{13}$$

Here, we normalize the interaction energy to one water molecule to allow for a better comparison between the clusters of different size. The interaction energy obtained from a supermolecular calculation of $E_{\text{tot}}$ can be used as reference, and is compared to the interaction energy per molecule from eb-MBEs of different orders, that is

$$E_{\text{int,eb-MBE}}^{(n)} = \frac{1}{N}\left(E_{\text{eb-MBE}}^{(n)} - E_{\text{eb,iso}}^{(1)}\right), \tag{14}$$

with the truncation error per molecule of the MBE

$$\Delta_{\text{eb-MBE}}^{(n)} = \frac{1}{N}\left(E_{\text{eb-MBE}}^{(n)} - E_{\text{supermol}}\right). \tag{15}$$

All calculations have been performed using DFT with the BP86 xc-functional[83,84] and a triple-zeta plus polarization (TZP) basis set of Slater-type orbitals[85] (see section "Computational Details" for further information).

Table 2 collects the interaction energies per molecule as well as the corresponding truncation errors (compared to the supermolecular reference calculation) at different orders of eb-MBEs for $(H_2O)_5$ and $(H_2O)_{17}$. In addition to the isolated eb-MBE, two different embedded eb-MBEs

**TABLE 2** Interaction energies per molecular fragment (in kJ/mol) of the water clusters $(H_2O)_5$ and $(H_2O)_{17}$ obtained from energy-based many-body expansions compared to the supermolecular reference value for DFT/BP86/TZP calculations

| | | Iso | | PC | | FDE | |
|---|---|---|---|---|---|---|---|
| | Order | $E^{(n)}_{\text{int,eb-MBE}}$ | $\Delta^{(n)}$ | $E^{(n)}_{\text{int,eb-MBE}}$ | $\Delta^{(n)}$ | $E^{(n)}_{\text{int,eb-MBE}}$ | $\Delta^{(n)}$ |
| $(H_2O)_5$ | Two-body | −9.45 | +1.40 | −10.16 | +0.69 | −9.97 | +0.88 |
| | Three-body | −10.93 | −0.08 | −10.89 | −0.04 | −10.92 | −0.07 |
| | Four-body | −10.86 | −0.01 | −10.86 | +0.01 | −10.85 | 0.00 |
| | Supermol. | −10.85 | | −10.85 | | −10.85 | |
| $(H_2O)_{17}$ | Two-body | −11.12 | +2.37 | −11.95 | +1.54 | −11.79 | +1.70 |
| | Three-body | −13.66 | −0.17 | −13.66 | −0.17 | −13.71 | −0.22 |
| | Four-body | −13.63 | −0.14 | −13.60 | −0.11 | −13.36 | +0.13 |
| | Supermol. | −13.49 | | −13.49 | | −13.49 | |

*Note:* Included are the isolated eb-MBE (iso) as well as embedded eb-MBEs using point-charge embedding (PC) as well as frozen-density embedding (FDE). See text for details.

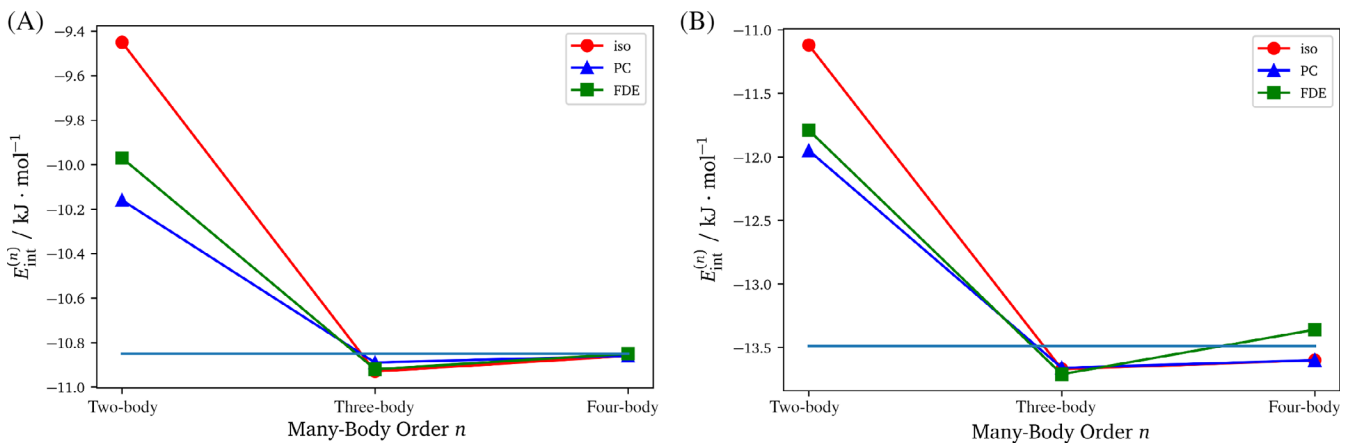


**FIGURE 2** Convergence of the energy-based many-body expansion for the interaction energies per molecular fragment, $E^{(n)}_{\text{int,eb-MBE}}$ (in kJ/mol) of, A, $(H_2O)_5$ and, B, $(H_2O)_{17}$ for DFT/BP86/TZP calculations. Included are the isolated eb-MBE (iso, red circles) as well as embedded eb-MBEs using point-charge embedding (PC, blue triangles) as well as frozen-density embedding (FDE, green squares). The supermolecular reference values are included as the horizontal line. See text for details

are considered. First, a conventional electrostatic PCE is used, in which TIP3P[86] point charges ($q_H$ = +0.417 and $q_O$ = −0.834) are assigned to the environment water molecules. Second, FDE is employed. Here we use the densities calculated for the isolated monomer subsystems to approximate the electron densities of the environment subsystems $\rho_K$ in Equation (12). Note that an iterative update of all subsystem densities in freeze-and-thaw iterations[26,87] would also be possible, but is not performed here. The results for the different eb-MBEs are also shown in Figure 2.

For the water pentamer, all eb-MBEs show the expected convergence toward the supermolecular result with increasing order of the MBE. In all cases, the supermolecular result is already reproduced with a four-body expansion, and the four-body contribution is below 0.1 kJ/mol per molecule. The truncation error of the two-body expansion (ie, the contribution of three-body and higher order terms) amounts to 1.40 kJ/mol per molecule for the isolated eb-MBE. This truncation error is reduced to 0.69 and 0.88 kJ/mol per molecule for the embedded eb-MBEs with PCE and FDE, respectively. Similarly, the embedded MBEs also slightly reduce the truncation error of the three-body expansion (ie, the contribution of four-body and higher order terms).

A similar picture is obtained for $(H_2O)_{17}$, even though the truncation error per molecule is now larger than for the pentamer. With the isolated eb-MBE, the two-body truncation error amounts to 2.36 kJ/mol per molecule, which is reduced to 1.54 and 1.70 kJ/mol per molecule for the embedded eb-MBE with PCE and FDE, respectively. All eb-MBEs show a three-body truncation error between −0.17 and −0.22 kJ/mol per molecule and a four-body truncation error between −0.11 and +0.13 kJ/mol per molecule.

Altogether, our tests for two water clusters confirm that (a) three-body (and possibly also four-body) contributions are essential for describing many-body polarization effects and cannot be neglected in the eb-MBE[38,72] and (b) the truncation error (at least for the two-body expansion) of the eb-MBE can be reduced using a suitable embedding scheme.[71,72] However, for the embedded eb-MBEs, the two-body truncation error remains sizable and three-body contributions thus cannot be neglected: that is, overall the *n*-body convergence of the eb-MBE is not accelerated. This holds both for PCE and for FDE. This is in line with the previous finding that for water clusters, the embedded eb-MBE is rather insensitive to the choice of the embedding charges.[40,72,88]

## 2.4 | Many-body expansion of the electron density

In the embedded MBE, the embedding potential accounts for the polarization of the considered subsystems due to their environment. By inspecting the electron density, it becomes possible to directly judge the accuracy of the considered embedding schemes. Therefore, we consider the many-body expansion of the total electron density as (cf. Equations (1) and (4))

$$\begin{aligned}\rho_{\text{tot}}(\boldsymbol{r}) &= \sum_I \rho_I^{(1)}(\boldsymbol{r}) + \sum_{I<J} \Delta\rho_{IJ}^{(2)}(\boldsymbol{r}) + \sum_{I<J<K} \Delta\rho_{IJK}^{(3)}(\boldsymbol{r}) + \cdots \\ &= \rho_{\text{tot}}^{(1)}(\boldsymbol{r}) + \Delta\rho_{\text{tot}}^{(2)}(\boldsymbol{r}) + \Delta\rho_{\text{tot}}^{(3)}(\boldsymbol{r}) + \cdots = \rho_{\text{tot}}^{(1)}(\boldsymbol{r}) + \sum_{i=2}^{N} \Delta\rho_{\text{tot}}^{(i)}(\boldsymbol{r}),\end{aligned} \tag{16}$$

where all terms are defined in analogy to the MBE of the total energy. For instance, the two-body density corrections are defined as $\Delta\rho_{IJ}^{(2)} = \rho_{IJ} - \rho_I^{(1)} - \rho_J^{(1)}$ and the three-body density corrections are given by $\Delta\rho_{IJK}^{(3)} = \rho_{IJK} - \Delta\rho_{IJ}^{(2)} - \Delta\rho_{IK}^{(2)} - \Delta\rho_{JK}^{(2)} - \rho_I^{(1)} - \rho_J^{(1)} - \rho_K^{(1)}$. As for the total energy, the MBE can be performed using calculations for isolated or embedded subsystems, and the total electron density can be approximated by a truncated MBE:

$$\rho_{\text{tot}}(\mathbf{r}) \approx \rho_{\text{tot}}^{(n)}(\mathbf{r}) = \rho_{\text{tot}}^{(1)}(\mathbf{r}) + \sum_{i=2}^{n} \Delta\rho_{\text{tot}}^{(i)}(\mathbf{r}). \tag{17}$$

To assess the convergence of the isolated and embedded MBEs for the electron density, Figure 3 shows isosurface plots of the difference densities of the many-body expanded electron densities compared to the ones obtained from a supermolecular calculation

$$\Delta\rho_{\text{MBE}}^{(n)}(\boldsymbol{r}) = \rho_{\text{tot}}(\boldsymbol{r}) - \rho_{\text{tot}}^{(n)}(\boldsymbol{r}) \tag{18}$$

for the test case of the water pentamer. For a quantitative assessment, the integrated density errors

$$\left|\Delta\rho_{\text{MBE}}^{(n)}\right| = \int \left|\rho_{\text{tot}}(\boldsymbol{r}) - \rho_{\text{tot}}^{(n)}(\boldsymbol{r})\right| \mathrm{d}^3 r \tag{19}$$

are listed in Table 3 for the different MBEs of the electron density in both the water pentamer and $(H_2O)_5$.

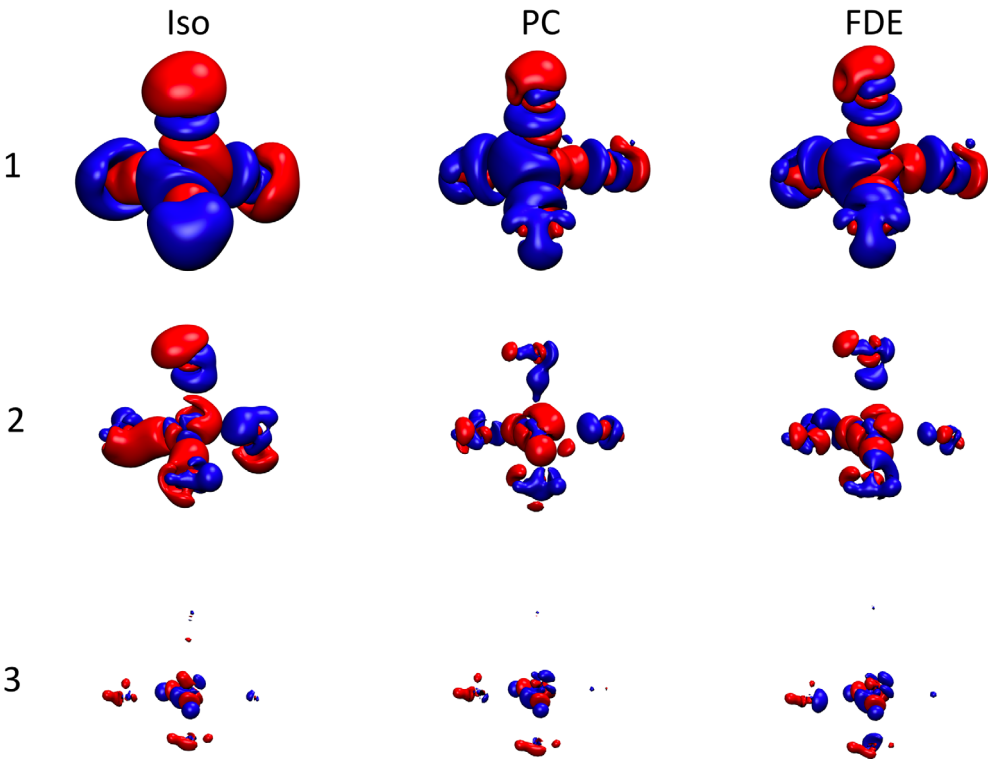


**FIGURE 3** Isosurface plots (isovalue $2.0 \times 10^{-4}$ e/bohr$^3$ for one-body and $0.7 \times 10^{-4}$ e/bohr$^3$ for two-body and three-body expansion) of the truncation error in the total electron density $\Delta\rho_{\text{MBE}}^{(n)}(r)$ (see Equation (18)) at different orders $n$ of the isolated MBE (iso) and of embedded MBEs using point-charge embedding (PC) and frozen-density embedding (FDE) for $(H_2O)_5$. With a four-body expansion, the difference densities are not visible anymore with the chosen isovalue

| | $(H_2O)_5$ | | | $(H_2O)_{17}$ | | |
|---|---|---|---|---|---|---|
| | iso | PC | FDE | iso | PC | FDE |
| One-body | 0.455 | 0.196 | 0.183 | 1.759 | 0.774 | 0.713 |
| Two-body | 0.040 | 0.020 | 0.020 | 0.194 | 0.094 | 0.098 |
| Three-body | 0.006 | 0.005 | 0.006 | 0.075 | 0.065 | 0.065 |
| Four-body | 0.001 | 0.001 | 0.001 | 0.071 | 0.069 | 0.068 |

*Note:* All values in $e$/bohr$^3$.

**TABLE 3** Integrated density errors in the total electron density $\left|\Delta\rho_{\mathrm{MBE}}^{(n)}\right|$ (see Equation (19)) at different orders $n$ of the isolated MBE (iso) and of embedded MBEs using point-charge embedding (PC) and frozen-density embedding (FDE) for $(H_2O)_5$ and $(H_2O)_{17}$

Inspection of Figure 3 shows that for $(H_2O)_5$, the convergence of the total density is significantly accelerated with the embedded MBEs compared to the isolated MBEs. Already at first order (ie, for the sum of the fragment densities) the inclusion of an embedding potential significantly improves the electron density. Similarly, for a two-body expansion the difference densities obtained from the embedded MBEs are considerably smaller than for the isolated MBE. For three-body and four-body expansions, the difference densities approach zero for both the isolated and the embedded MBEs. These observations are confirmed by the integrated density errors listed in Table 3. At first and second order, the density error of the embedded MBEs is less than half of that obtained in the isolated MBE, while for the three-body and four-body expansions very small errors of similar size are obtained in all cases. Similar observations can be made for $(H_2O)_{17}$. At first and second order, the embedded MBEs reduce the density error by more than half. For the three-body and four-body expansions, the embedded MBEs still improve the electron densities compared to the isolated MBE, but to a smaller extent. Note that for $(H_2O)_{17}$, the density errors in the four-body expansion is still larger than for $(H_2O)_5$, which is explained by the larger number of nearest neighbor interactions (ie, in the 17-mer, the five central water molecules are each coordinated to four other water molecules).

Thus, with embedded MBEs the electron density can already be considered converged with a two-body expansion, and three-body and higher order contributions become negligible for the electron density ($|\Delta\rho_{\mathrm{MBE}}{}^{(n)}| < 0.1$) if an embedded MBE is used. This is in stark contrast to the slower convergence that was observed for the interaction energies. Finally, we note that, as for the interaction energies, the use of an FDE potential does not significantly improve upon the use of TIP3P PCE for the considered water clusters.

## 3 | DENSITY-BASED MANY-BODY EXPANSION

### 3.1 | Theory

The observation that an embedded many-body expansion converges significantly faster for the electron density than for the energy led us to the idea to exploit this faster convergence by performing a density-based MBE of the total energy as

$$E_{\mathrm{tot}} = E_{\mathrm{tot}}\left[\sum_I \rho_I^{(1)}(\boldsymbol{r}) + \sum_{I<J}\Delta\rho_{IJ}^{(2)}(\boldsymbol{r}) + \sum_{I<J<K}\Delta\rho_{IJK}^{(3)}(\boldsymbol{r}) + \cdots\right], \tag{20}$$

that is, to use the many-body expanded density in the DFT total energy expression (cf. Equation (5)). By truncating the MBE of the total electron density (cf. Equation (17)), one obtains a truncated density-based MBE (db-MBE) that can be used to approximate the total energy:

$$E_{\mathrm{tot}} \approx E_{db}^{(n)} = E_{\mathrm{tot}}\left[\rho_{\mathrm{tot}}^{(n)}(\boldsymbol{r})\right]. \tag{21}$$

Given the results of the previous section, it can be expected that this db-MBE converges faster with respect to the many-body expansion order than the conventional eb-MBE. As will be shown below, the total energy of a truncated db-MBE can be expressed as the total energy of the corresponding eb-MBE plus an interaction energy correction

$$E_{db}^{(n)} = E_{\mathrm{tot}}\left[\rho_{\mathrm{tot}}^{(n)}(\boldsymbol{r})\right] = E_{eb}^{(n)} + E_{\mathrm{corr}}^{(n)}. \tag{22}$$

When including only the first-order contribution to the total density (ie, the total electron density is approximated as a sum of fragment densities), Equation (20) leads to the one-body energy in the db-MBE

$$\begin{aligned} E_{\mathrm{db}}^{(1)} &= E_{\mathrm{tot}}\left[\sum_I \rho_I^{(1)}\right] = \sum_I T_s\left[\rho_I^{(1)}\right] + \sum_I \int \rho_I^{(1)}(\boldsymbol{r}) v_{\mathrm{nuc}}^{(I)}(\boldsymbol{r}) \mathrm{d}^3 r + \sum_I J\left[\rho_I^{(1)}\right] \\ &+ \sum_I E_{\mathrm{xc}}\left[\rho_I^{(1)}\right] + \sum_I E_{\mathrm{NN}}^{(II)} + \sum_{I\neq J} \int \rho_I^{(1)}(\boldsymbol{r}) v_{\mathrm{nuc}}^{(J)}(\boldsymbol{r}) \mathrm{d}^3 r \\ &+ \sum_{I<J} \int\int \frac{\rho_I^{(1)}(\boldsymbol{r}) \rho_J^{(1)}(\boldsymbol{r}')}{|\boldsymbol{r}-\boldsymbol{r}'|} \mathrm{d}^3 r \mathrm{d}^3 r' + \sum_{I<J} E_{\mathrm{NN}}^{(IJ)} \\ &+ T_s^{\mathrm{nadd}}\left[\left\{\rho_I^{(1)}\right\}\right] + E_{\mathrm{xc}}^{\mathrm{nadd}}\left[\left\{\rho_I^{(1)}\right\}\right] \end{aligned} \tag{23}$$

where the nonadditive kinetic and xc energy functionals are defined as

$$T_s^{\mathrm{nadd}}\left[\left\{\rho_I^{(1)}\right\}\right] = T_s\left[\sum_I \rho_I^{(1)}\right] - \sum_I T_s\left[\rho_I^{(1)}\right] \tag{24}$$

$$E_{\mathrm{xc}}^{\mathrm{nadd}}\left[\left\{\rho_I^{(1)}\right\}\right] = E_{\mathrm{xc}}\left[\sum_I \rho_I^{(1)}\right] - \sum_I E_{\mathrm{xc}}\left[\rho_I^{(1)}\right]. \tag{25}$$

This one-body energy can be decomposed as

$$E_{\mathrm{db}}^{(1)} = \sum_I E_I + E_{\mathrm{corr}}^{(1)} = E_{\mathrm{eb}}^{(1)} + E_{\mathrm{corr}}^{(1)}, \tag{26}$$

with the one-body energy in the eb-MBE

$$E_{\mathrm{eb}}^{(1)} = \sum_I E_I\left[\rho_I^{(1)}\right] \tag{27}$$

and an interaction energy correction

$$\begin{aligned} E_{\mathrm{corr}}^{(1)} &= \sum_{I\neq J} \int \rho_I^{(1)}(\boldsymbol{r}) v_{\mathrm{nuc}}^{(J)}(\boldsymbol{r}) \mathrm{d}^3 r + \sum_{I<J} \int\int \frac{\rho_I^{(1)}(\boldsymbol{r}) \rho_J^{(1)}(\boldsymbol{r}')}{|\boldsymbol{r}-\boldsymbol{r}'|} \mathrm{d}^3 r \mathrm{d}^3 r' + \sum_{I<J} E_{\mathrm{NN}}^{(IJ)} \\ &+ E_{\mathrm{xc}}^{\mathrm{nadd}}\left[\left\{\rho_I^{(1)}\right\}\right] + T_s^{\mathrm{nadd}}\left[\left\{\rho_I^{(1)}\right\}\right], \end{aligned} \tag{28}$$

where the nonadditive kinetic and xc energy contributions need to be evaluated using an approximate functional that depends only on the local electron density (eg, GGA-type functionals[75,76]), as is common in subsystem DFT.[12] If the electron densities $\rho_I^{(1)}$ are obtained from calculations for the isolated fragments, the above energy expressions are equivalent to the Harris functional,[89,90] whereas for electron densities obtained in the presence of an potential, they correspond to those used in FDE theory and subsystem DFT.[12,63,91] Note, however, that the electron densities are not determined self-consistently and thus do not minimize the energy functional of Equation (23).

Even though we used the formalism of DFT to derive the above energy expressions, the above interaction energy correction $E_{\mathrm{corr}}^{(1)}$ can be combined with energies $E_{\mathrm{eb}}^{(1)}$ obtained from the MBE with any QC method. The evaluation of the interaction energy correction according to Equation (28) requires only the fragment electron densities, which are also available from both DFT and wavefunction-based QC methods.

When going beyond first order in db-MBE, we still want to express the total energy as the sum of the energy of the truncated eb-MBE and an interaction energy correction $E_{\mathrm{corr}}^{(n)}$ (cf. Equation (22)). To obtain an expression for $E_{\mathrm{corr}}^{(n)}$, we first realize that, within the DFT formalism, the total energy is the sum of five energy contributions, and an eb-MBE can be performed for each of these terms separately. Therefore, in a truncated $n$-body expansion, each of these terms ($X = T_s$, $V_{\mathrm{nuc}}$, $J$, $E_{\mathrm{xc}}$, $E_{\mathrm{NN}}$) is approximated as

$$X^{(n)} = X^{(1)} + \sum_{i=2}^{n} \Delta X^{(n)}. \tag{29}$$

Thus, the total energy in the truncated eb-MBE can be expressed as

$$\begin{aligned} E_{\mathrm{eb}}^{(n)} &= T_s^{(n)} + V_{\mathrm{nuc}}^{(n)} + J^{(n)} + E_{\mathrm{xc}}^{(n)} + E_{\mathrm{NN}}^{(n)} \\ &= E^{(1)} + \sum_{i=1}^{n} \left(\Delta T_s^{(n)} + \Delta V_{\mathrm{nuc}}^{(n)} + \Delta J^{(n)} + \Delta E_{\mathrm{xc}}^{(n)}\right) + \Delta E_{\mathrm{NN}}^{(2)} \end{aligned} \tag{30}$$

Note that for the nuclear-nuclear repulsion energy, which is independent of the electron density, there are only up to two-body contributions.

By rearranging Equation (21) and using the eb-MBE of the different energy contributions (see Equation (29)), we find that for $n > 1$ the $n$-body interaction energy correction is given by

$$\begin{aligned} E_{\mathrm{corr}}^{(n)} &= E_{\mathrm{tot}}\left[\rho_{\mathrm{tot}}^{(n)}(\boldsymbol{r})\right] - E_{\mathrm{eb}}^{(n)} \\ &= \left(V_{\mathrm{nuc}}\left[\rho_{\mathrm{tot}}^{(n)}\right] - V_{\mathrm{nuc}}^{(n)}\right) + \left(J\left[\rho_{\mathrm{tot}}^{(n)}\right] - J^{(n)}\right) \\ &\quad + T_s^{\mathrm{nadd},(n)}[\{\rho_I\},\{\rho_{IJ}\},\ldots] + E_{\mathrm{xc}}^{\mathrm{nadd},(n)}[\{\rho_I\},\{\rho_{IJ}\},\ldots] \end{aligned} \tag{31}$$

Here, the $n$-body nonadditive kinetic and xc energy functionals are defined as

$$T_s^{\mathrm{nadd},(n)}[\{\rho_I\},\{\rho_{IJ}\},\ldots] = T_s\left[\rho_{\mathrm{tot}}^{(n)}\right] - T_s^{(n)} \tag{32}$$

$$E_{\mathrm{xc}}^{\mathrm{nadd},(n)}[\{\rho_I\},\{\rho_{IJ}\},\ldots] = E_{\mathrm{xc}}\left[\rho_{\mathrm{tot}}^{(n)}\right] - E_{\mathrm{xc}}^{(n)}. \tag{33}$$

Again, these contributions need to be evaluated using suitable approximate density functionals.[12,75,76]

The electron-nuclei attraction energy functional $V_{\mathrm{nuc}}\left[\rho_{\mathrm{tot}}^{(n)}\right]$ and the Coulomb repulsion energy functional $J\left[\rho_{\mathrm{tot}}^{(n)}\right]$ can be evaluated recursively for the many-body expanded electron density. For the electron-nuclei attraction energy, we find

$$V_{\mathrm{nuc}}\left[\rho_{\mathrm{tot}}^{(n)}\right] = V_{\mathrm{nuc}}\left[\rho_{\mathrm{tot}}^{(n-1)} + \Delta\rho_{\mathrm{tot}}^{(n)}\right] = V_{\mathrm{nuc}}\left[\rho_{\mathrm{tot}}^{(n-1)}\right] + \int \Delta\rho_{\mathrm{tot}}^{(n)} v_{\mathrm{nuc}}(\boldsymbol{r})\mathrm{d}^3r, \tag{34}$$

and for the Coulomb energy we have

$$\begin{aligned} J\left[\rho_{\mathrm{tot}}^{(n)}\right] &= J\left[\rho_{\mathrm{tot}}^{(n-1)} + \Delta\rho_{\mathrm{tot}}^{(n)}\right] \\ &= J\left[\rho_{\mathrm{tot}}^{(n-1)}\right] + \int\int \frac{\rho_{\mathrm{tot}}^{(n-1)}(\boldsymbol{r})\Delta\rho_{\mathrm{tot}}^{(n)}(\boldsymbol{r}')}{|\boldsymbol{r}-\boldsymbol{r}'|}\mathrm{d}^3r\mathrm{d}^3r' + \frac{1}{2}\int\int \frac{\Delta\rho_{\mathrm{tot}}^{(n)}(\boldsymbol{r})\Delta\rho_{\mathrm{tot}}^{(n)}(\boldsymbol{r}')}{|\boldsymbol{r}-\boldsymbol{r}'|}\mathrm{d}^3r\mathrm{d}^3r'. \end{aligned} \tag{35}$$

Thus, for $n > 1$, the calculation of these corrections requires only the knowledge of the total electron density at expansion order $n - 1$ and the $n$-body correction to the total electron density. Similarly, the calculation of $T_s^{\mathrm{nadd},(n)}$ and $E_{\mathrm{xc}}^{\mathrm{nadd},(n)}$ requires only the electron densities from subsystem calculations. Further details of our implementation are given in "Computational Details." As they require only the knowledge of electron densities, all contributions to $E_{\mathrm{corr}}^{(n)}$ are accessible both in DFT and in wavefunction-based QC calculations. Moreover, all subsystem calculations can be performed either for isolated or for embedded subsystems without affecting the calculation of $E_{\mathrm{corr}}^{(n)}$. Thus, a db-MBE as introduced here can be consistently combined with any MBE strategy without introducing issues due to possible double counting.

## 3.2 | Test case: Water clusters

For a first test of the accuracy of density-based MBEs, we return to the $(H_2O)_5$ and $(H_2O)_{17}$ water clusters considered previously. Table 4 lists the interaction energies per molecule obtained with truncated db-MBEs at different expansion orders. These values can be directly compared to those in Table 2 for eb-MBEs. The many-body convergence of the energy-based and density-based MBEs is also shown in Figure 4.

Whereas in the eb-MBE at least a two-body expansion is required to approximate the interaction energy in a molecular cluster, the db-MBE already provides a reasonable estimate at first order: that is, using only the QC calculation performed for the monomers. For the isolated db-MBE, the energy difference to the full supermolecular calculation amounts to 2.69 kJ/mol per fragment for $(H_2O)_5$ and 3.69 kJ/mol per fragment $(H_2O)_{17}$. However, for the embedded db-MBEs the error of the one-body db-MBE is below 1.1 kJ/mol per fragment for both test cases. This error is comparable to or even smaller than that of the two-body eb-MBE.

For $(H_2O)_5$, the error in the interaction energy amounts to 0.41 kJ/mol per fragment for the isolated db-MBE and to less than 0.3 kJ/mol per fragment for the embedded db-MBEs. For the db-MBE, this is only a third of the truncation error of the eb-MBE, while for the embedded db-MBEs the error is reduced to less than half. For the three-body db-MBE, the remaining error in the interaction energy is <0.1 kJ/mol per fragment, which is similar to the truncation error of the corresponding three-body eb-MBEs.

For $(H_2O)_{17}$, the two-body db-MBE predicts the interaction energy within 0.65 kJ/mol for both the isolated and the embedded cases. Compared to the two-body eb-MBE, this corresponds to a reduction to almost a fourth in the isolated MBE and to approximately a third in the

**TABLE 4** Interaction energies per molecular fragment (in kJ/mol) of the water clusters $(H_2O)_5$ and $(H_2O)_{17}$ obtained from density-based many-body expansions compared to the supermolecular reference value for DFT/BP86/TZP calculations

| | | iso | | PC | | FDE | |
|---|---|---|---|---|---|---|---|
| | Order | $E^{(n)}_{\text{int,db-MBE}}$ | $\Delta^{(n)}$ | $E^{(n)}_{\text{int,db-MBE}}$ | $\Delta^{(n)}$ | $E^{(n)}_{\text{int,db-MBE}}$ | $\Delta^{(n)}$ |
| $(H_2O)_5$ | One-body | −8.16 | +2.69 | −11.67 | −0.82 | −11.86 | −1.01 |
| | Two-body | −11.26 | −0.41 | −11.11 | −0.26 | −11.14 | −0.29 |
| | Three-body | −10.74 | +0.09 | −10.77 | +0.08 | −10.76 | +0.09 |
| | Four-body | −10.85 | 0.00 | −10.86 | −0.01 | −10.86 | −0.01 |
| | Supermol. | −10.85 | | −10.85 | | −10.85 | |
| $(H_2O)_{17}$ | One-body | −9.80 | +3.69 | −14.36 | −0.87 | −14.56 | −1.07 |
| | Two-body | −14.14 | −0.65 | −13.99 | −0.50 | −14.07 | −0.58 |
| | Three-body | −13.20 | +0.29 | −13.17 | +0.32 | −13.18 | +0.31 |
| | Four-body | −13.74 | −0.25 | −13.74 | −0.25 | −13.72 | −0.23 |
| | Supermol. | −13.49 | | −13.49 | | −13.49 | |

*Note:* Included are the isolated db-MBE (iso) as well as embedded db-MBEs using point-charge embedding (PC) and frozen-density embedding (FDE). See text for details.

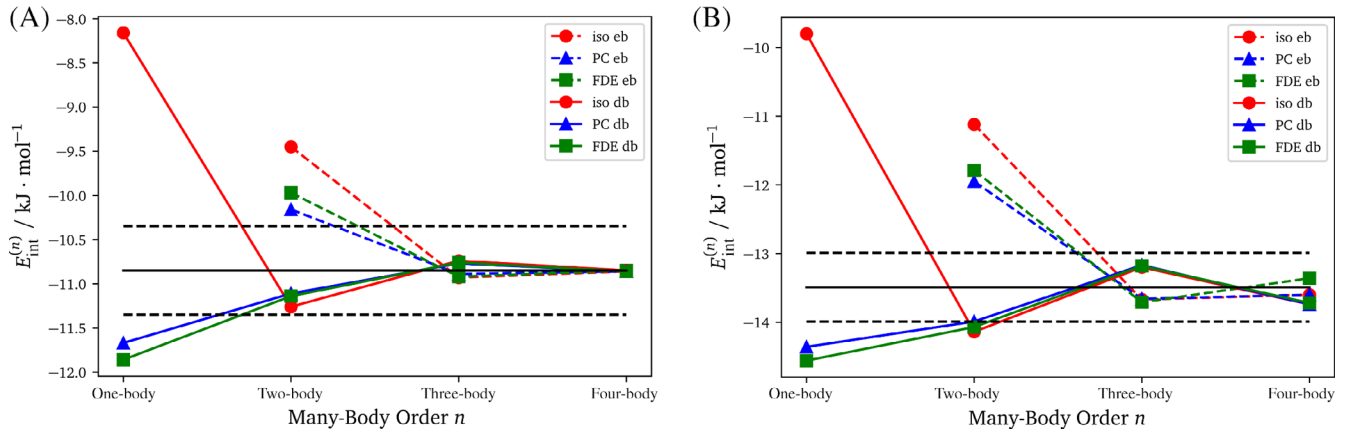


**FIGURE 4** Convergence of the density-based many-body expansion for the interaction energies per molecular fragment, $E^{(n)}_{\text{int,db-MBE}}$ (in kJ/mol) of, A, $(H_2O)_5$ and, B, $(H_2O)_{17}$ for DFT/BP86/TZP calculations. Included are results for the db-MBE (solid lines) using isolated subsystems (iso, red circles) as well as point-charge embedding (PC, blue triangles) and frozen-density embedding (FDE, green squares). The interaction energies obtained with energy-based MBEs (dashed lines, cf. Figure 2) are included for comparison. The supermolecular reference values are included as a solid horizontal line, whereas the dashed horizontal lines indicate a target accuracy of 0.5 kJ/mol per fragment. See text for details

embedded MBEs. For the three-body db-MBE, the error amounts to ∼0.3 kJ/mol per fragment in all cases, which is comparable to the truncation error of the corresponding three-body eb-MBEs. It is interesting to note that, when comparing the results for $(H_2O)_5$ and $(H_2O)_{17}$, in the eb-MBE the truncation error per fragment seems to increase roughly linearly with the number of fragments. Contrarily, for the one-body db-MBE the errors per fragment are similar for both cluster sizes, and for the two-body db-MBE only a slight increase of the error per fragment is observed for the larger cluster.

The visualization of the above data in Figure 4 demonstrates that to obtain interaction energies of similar (or even better) accuracy, db-MBE accelerates the convergence of the MBE by one order. While with the eb-MBE, a three-body expansion is required to reach a target accuracy of 0.5 kJ/mol per fragment, with the db-MBE a two-body expansion is already sufficient. In the case of $(H_2O)_{17}$, this corresponds to saving 680 QC calculations for trimers, which altogether require substantial computational effort.

## 3.3 | Test case: Aspirin clusters

As another test case, we consider molecular clusters of 2-acetoxybenzoic acid (aspirin). Aspirin crystallizes in two different polymorphs, dubbed form I and form II.[92] These are almost isoenergetic, which makes the computational prediction of the energy differences between the two

polymorphs a challenging test case.[93] Here, we consider two clusters of 16 aspirin molecules constructed as $2 \times 2$ supercells of the crystals structures of form I and form II (see Figure 5). The crystal structures have been obtained from the Cambridge Crystallographic Data Centre (CCDC) with reference codes ACSALA14 (form I) and ACSALA15 (form II).

While in the water clusters the intermolecular interactions are dominated by hydrogen bonding, in these aspirin clusters different types of intermolecular interactions, including hydrogen bonding, $\pi$-$\pi$ stacking, dipole-dipole interaction, dipole-$\pi$ interactions, and dispersion interactions, are competing. Note that while our aspirin form I cluster contains four hydrogen-bonded dimers, our form II cluster only contains two hydrogen-bonded dimers. Here, we compare the interaction energies obtained with the different MBEs to the supermolecular reference calculation. All calculations are performed using DFT/BP86/TZP. We note that no dispersion correction is included in our calculations, but this does not affect the comparison of the truncated MBE and the supermolecular results.

The interaction energies calculated for the form I and form II aspirin clusters obtained with the isolated and frozen-density embedded eb-MBEs as well as db-MBEs up to two-body contributions are given in Table 5. These are compared to the interaction energies from the corresponding supermolecular calculations. Because only clusters of the same size are compared, we now show the total interaction energies instead of the interaction energies *per monomer* discussed for the water clusters. When using calculations for isolated subsystems, the eb-MBE truncated after two-body contributions results in a truncation error of 7.9 kJ/mol for form I and of 12.8 kJ/mol for form II. Using FDE in the subsystem calculations slightly improves the interaction energy for form I, but worsens the result for form II.

With the db-MBE, the one-body expansion (ie, using only the calculations for monomers) provides a first estimate of the interaction energies, but with sizable error between +72.8 and −126.7 kJ/mol both for the isolated and the frozen-density embedded case. These can be attributed to the shortcoming of the employed nonadditive kinetic energy functional for weak intermolecular interactions.[94,95] When including two-body terms in the isolated db-MBE, the errors in the interaction energies are reduced to 0.6 kJ/mol for form I and 2.3 kJ/mol for form II; that is, the accuracy improves by more than a factor of five compared to the isolated eb-MBE. Altogether, the error of the two-body iso-db-MBE is below

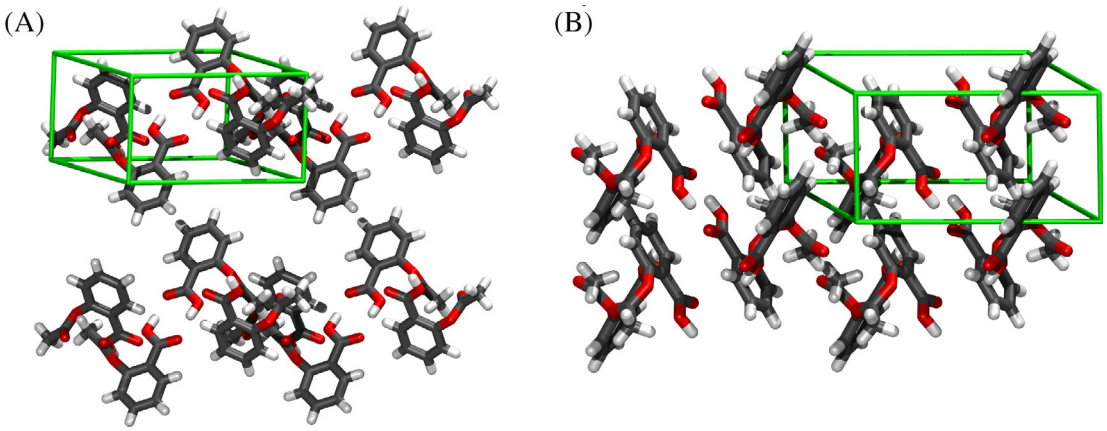


**FIGURE 5** Structures of clusters of 16 aspirin molecules extracted from the crystal structures of, A, form I and, B, form II. The unit cell is shown in green, and the considered clusters correspond to $2 \times 2$ supercells

**TABLE 5** Interaction energies (in kJ/mol) for the clusters of 16 aspirin molecules cut from the crystal structures of form I and form II obtained from energy-based as well as density-based many-body expansions compared to the supermolecular reference value for DFT/BP86/TZP calculations

| | | Energy-based | | | | Density-based | | | |
|---|---|---|---|---|---|---|---|---|---|
| | | iso | | FDE | | iso | | FDE | |
| | Order | $E_{\text{int}}^{(n)}$ | $\Delta^{(n)}$ | $E_{\text{int}}^{(n)}$ | $\Delta^{(n)}$ | $E_{\text{int}}^{(n)}$ | $\Delta^{(n)}$ | $E_{\text{int}}^{(n)}$ | $\Delta^{(n)}$ |
| Form I | One-body | | | | | −136.9 | +72.8 | −272.4 | −62.7 |
| | Two-body | −201.9 | +7.9 | −203.4 | +6.4 | −210.7 | −1.0 | −213.2 | −3.5 |
| | Supermol. | −209.8 | | −209.8 | | −209.8 | | −209.8 | |
| Form II | One-body | | | | | −58.7 | −12.8 | −172.6 | −126.7 |
| | Two-body | −33.1 | +12.7 | −31.0 | +14.8 | −47.9 | −2.1 | −51.5 | −5.7 |
| | Supermol. | −45.8 | | −45.8 | | −45.8 | | −45.8 | |

*Note*: Included are the isolated MBE (iso) as well as the frozen-density embedded (FDE) MBE. See text for details.

chemical accuracy for both aspirin clusters. For the frozen-density embedded db-MBE, the errors in the interaction energies of 3.5 kJ/mol for form I and 5.7 kJ/mol for form II are again significantly smaller than for the eb-MBE by approximately a factor of two. However, these are somewhat larger than for the iso-db-MBE. We attribute this to the lack of a self-consistent optimization of the subsystem electron densities.

## 4 | CONCLUSIONS

We have explored the combination of MBEs with quantum embedding methods. The MBE constitutes a fragmentation method for the QC treatment of large molecular clusters and crystals that systematically converges toward the exact supermolecular result. However, it becomes formally exact only if all *n*-body contributions up to the number of molecular fragments are included. A truncation at low order has to be applied to gain a computational advantage compared to a full supermolecular calculation. However, this truncation inevitably introduces an error. On the other hand, quantum embedding methods and related QC subsystem methods are in principle able to provide the exact supermolecular result from the fragment calculations (ie, including only one-body terms). However, to be computationally feasible, all such methods introduce approximations of some sort, and their accuracy might be difficult to predict.

In this work, we have combined these two complementary approaches, that is, the systematically improvable truncated MBE with the formally exact subsystem DFT and FDE theory. First, we applied FDE for including the effect of the environment into the subsystem calculations necessary in FDE. We found that for water clusters, this could reduce the errors in the interaction energy for an eb-MBE truncated at low order compared to the use of calculations for the isolated subsystems. However, using FDE hardly improves upon the classical PCE. Furthermore, for the test case of aspirin clusters, no benefits of frozen-density embedded subsystem calculations were found compared to the isolated eb-MBE.

However, we found that the use of a suitable embedding potential in the subsystem calculations significantly improves the convergence of an MBE for the electron density. In fact, with the exact FDE potential, already a one-body expansion (ie, the sum of fragment densities) would reproduce the correct supermolecular density. With an approximate embedding potential, we found that the embedded MBE converges rapidly for the electron density, and already a two-body expansion is often sufficiently accurate.

A further analysis shows that even if the MBE of the electron density converged, the conventional eb-MBE would not yield the exact supermolecular energy. At first order, the eb-MBE misses the interaction between the monomer electron densities, while at second order it misses the interaction of the dimer corrections, $\Delta\rho_{IJ}$, with the electron densities of the other subsystems. This can be alleviated with the db-MBE introduced in the present work. By inserting the many-body expanded electron density into the total energy functional, it becomes possible to exploit the rapid convergence of the MBE for the electron density to improve the energies obtained from the eb-MBE.

We found that the use of a db-MBE could accelerate the many-body convergence by one order compared to the eb-MBE. For our test cases, accurate interaction energies could be obtained from a db-MBE including only one- and two-body terms. For the considered water clusters, the errors in the interaction energies are below 1 kJ/mol per fragment, whereas they are smaller than 4 kJ/mol for the considered clusters of 16 aspirin molecules. With eb-MBE, the inclusion of three-body terms is mandatory to achieve such an accuracy. As the benchmarks presented here are limited, we plan to present more comprehensive tests of the accuracy of db-MBEs elsewhere.

Conceptually, there are two different perspectives on the db-MBE. First, it can be viewed as an ONIOM-style composite method,[56–58] in which a truncated MBE using a suitable QC method is used as a high-level method while an orbital-free DFT treatment using an approximate kinetic energy functional is used as low-level method (cf. Klüner[96]). Thus, compared to other composite schemes based on a truncated MBE,[59–62] the use of, for example, a polarizable force field for approximating the neglected many-body contributions is replaced by an interaction energy correction that depends on the subsystems' electron densities. Second, the db-MBE can be viewed as an extension of subsystem-DFT[12] that corrects for insufficiencies of approximate nonadditive kinetic energy functional by pairwise (and possibly higher order) corrections.

While here we only employed KS-DFT for the subsystem calculations within the db-MBE, the presented methodology can be combined with any QC method, including high-level wave function-based method. As the theory is formulated only in terms of the subsystem electron densities, it is particularly easy to combine with different QC methods and MBE strategies, without introducing problems due to a potential double counting of energy contributions. In combination with periodic density-based embedding schemes,[28,97] the db-MBE thus provides an intriguing approach for the accurate QC treatment of molecular crystals. In such applications, the use of accurate nonlocal kinetic energy functionals recently developed by Pavanello and coworkers[98,99] might be particularly promising.

## 5 | COMPUTATIONAL DETAILS

All QC calculations were performed using DFT as implemented in the Amsterdam Density-Functional (ADF) program package.[100,101] The BP86 xc-functional[83,84] and a triple-zeta plus polarization (TZP) basis set of Slater-type orbitals[85] were used throughout. All subsystem energies were obtained with ADF's total energy implementation.[94] To be sure to avoid numerical precision issues,[37] we used a Becke integration grid of "very good" accuracy.[102] For the FDE MBE calculations, we employed ADF's implementation of FDE.[103] To ensure all energy terms are obtained with

the required accuracy, the full supermolecular integration grid is used in all FDE calculations as well as for the evaluation of the interaction energy terms in the db-MBE. The PW91k nonadditive kinetic energy functional[104] was used where applicable.

To automate the subsystem calculations needed to perform eb-MBE, we utilized the PyADF scripting framework.[105] We implemented the additional interaction energy terms needed for the db-MBE in PyADF, making use of our recently developed PyEmbed module, which provides a stand-alone implementation of the subsystem DFT embedding potential and interaction energy terms. The *n*-body nonadditive xc and kinetic energy (see Equations (32) and (33)) were evaluated using the XCFun library.[106,107] The electrostatic interaction energies were calculated in PyEmbed by numerical integration from the electron densities and the nuclear and Coulomb potentials exported from ADF according to Equations (28), (34), and (35). Here, the necessary fit corrections are included as described in Refs. [94, 108].

We note that by using subsystem-specific grids instead of relying on the supermolecular integration grid in all steps, the performance of our current pilot implementation can be improved. In future work, we will explore these possibilities in order to provide an efficient implementation of density-based many-body expansions.

Cartesian coordinates of all molecular clusters used as test cases in this work are available at https://doi.org/10.26434/chemrxiv.11816739.

## ACKNOWLEDGMENTS

We are indebted to Dr André Severo Pereira Gomes (Laboratoire PhLAM, CNRS UMR 8523, and Université de Lille) for contributions to the development of PyEmbed. We further thank Roland Pollack (TU Braunschweig) for performing initial calculations at an early stage of this project.

## AUTHOR CONTRIBUTIONS

**Daniel Schmitt-Monreal:** Investigation; methodology; validation; visualization; writing-original draft; writing-review and editing. **Christoph Jacob:** Conceptualization; methodology; supervision; writing-original draft; writing-review and editing.

## ORCID

*Christoph R. Jacob* https://orcid.org/0000-0002-6227-8476

## REFERENCES

[1] M. S. Gordon, D. G. Fedorov, S. R. Pruitt, L. V. Slipchenko, *Chem. Rev.* **2012**, *112*, 632.
[2] S. R. Pruitt, C. Bertoni, K. R. Brorsen, M. S. Gordon, *Acc. Chem. Res.* **2014**, *47*, 2786.
[3] K. Raghavachari, A. Saha, *Chem. Rev.* **2015**, *115*, 5643.
[4] L. O. Jones, M. A. Mosquera, G. C. Schatz, M. A. Ratner, *J. Am. Chem. Soc.* **2020**, *142*, 3281.
[5] A. S. P. Gomes, C. R. Jacob, *Annu. Rep. Prog. Chem., Sect. C* **2012**, *108*, 222.
[6] A. Goez, J. Neugebauer, Embedding Methods in Quantum Chemistry. in *Frontiers of Quantum Chemistry* (Eds: M. J. Wójcik, H. Nakatsuji, B. Kirtman, Y. Ozaki), Springer, Singapore **2018**, p. 139. https://doi.org/10.1007/978-981-10-5651-2_7
[7] B. Mennucci, *WIREs Comput. Mol. Sci.* **2012**, *2*, 386.
[8] F. Lipparini, B. Mennucci, *J. Chem. Phys.* **2016**, *144*, 160901.
[9] H. M. Senn, W. Thiel, *Angew. Chem. Int. Ed.* **2009**, *48*, 1198.
[10] S. Ahmadi, L. B. Herrera, M. Chehelamirani, J. Hostaš, S. Jalife, D. R. Salahub, *Int. J. Quantum Chem.* **2018**, *118*, e25558.
[11] U. N. Morzan, D. J. Alonso de Armiño, N. O. Foglia, F. Ramírez, M. C. González Lebrero, D. A. Scherlis, D. A. Estrin, *Chem. Rev.* **2018**, *118*, 4071.
[12] C. R. Jacob, J. Neugebauer, *WIREs Comput. Mol. Sci.* **2014**, *4*, 325.
[13] F. Libisch, C. Huang, E. A. Carter, *Acc. Chem. Res.* **2014**, *47*, 2768.
[14] T. A. Wesolowski, S. Shedge, X. Zhou, *Chem. Rev.* **2015**, *115*, 5891.
[15] Q. Sun, G. K.-L. Chan, *Acc. Chem. Res.* **2016**, *49*, 2705.
[16] S. J. R. Lee, M. Welborn, F. R. Manby, T. F. Miller, *Acc. Chem. Res.* **2019**, *52*, 1359.
[17] J. Neugebauer, C. R. Jacob, T. A. Wesolowski, E. J. Baerends, *J. Phys. Chem. A* **2005**, *109*, 7805.
[18] R. E. Bulo, C. R. Jacob, L. Visscher, *J. Phys. Chem. A* **2008**, *112*, 2640.
[19] T. D. Crawford, A. Kumar, K. P. Hannon, S. Höfener, L. Visscher, *J. Chem. Theory Comput.* **2015**, *11*, 5305.
[20] C. König, J. Neugebauer, *Phys. Chem. Chem. Phys.* **2011**, *13*, 10475.
[21] J. Neugebauer, J. Veldstra, F. Buda, *J. Phys. Chem. B* **2011**, *115*, 3216.
[22] C. König, J. Neugebauer, *J. Chem. Theory Comput.* **2013**, *9*, 1808.
[23] S. J. Bennie, M. W. van der Kamp, R. C. R. Pennifold, M. Stella, F. R. Manby, A. J. Mulholland, *J. Chem. Theory Comput.* **2016**, *12*, 2689.
[24] X. Zhang, S. J. Bennie, M. W. van der Kamp, D. R. Glowacki, F. R. Manby, A. J. Mulholland, R. Soc, *Open Sci* **2018**, *5*, 171390.
[25] H. Jiang, M. Kammler, F. Ding, Y. Dorenkamp, F. R. Manby, A. M. Wodtke, T. F. Miller, A. Kandratsenka, O. Bünermann, *Science* **2019**, *364*, 379.
[26] P. Cortona, *Phys. Rev. B* **1992**, *46*, 2008.
[27] M. Iannuzzi, B. Kirchner, J. Hutter, *Chem. Phys. Lett.* **2006**, *421*, 16.
[28] A. Genova, D. Ceresoli, M. Pavanello, *J. Chem. Phys.* **2014**, *141*, 174101.
[29] M. Welborn, T. Tsuchimochi, T. Van Voorhis, *J. Chem. Phys.* **2016**, *145*, 074102.
[30] G. J. O. Beran, *Chem. Rev.* **2016**, *116*, 5567.
[31] S. Wen, G. J. O. Beran, *J. Chem. Theory Comput.* **2012**, *8*, 2698.
[32] J. Yang, W. Hu, D. Usvyat, D. Matthews, M. Schütz, G. K.-L. Chan, *Science* **2014**, *345*, 640.
[33] H. Stoll, H. Preuß, *Theor. Chim. Acta* **1977**, *46*, 11.

[34] I. G. Kaplan, *Theory of Molecular Interactions*, Elsevier, Amsterdam **1986**.
[35] K. Rościszewski, B. Paulus, P. Fulde, H. Stoll, *Phys. Rev. B* **1999**, *60*, 7905.
[36] J. Cui, H. Liu, K. D. Jordan, *J. Phys. Chem. B* **2006**, *110*, 18872.
[37] R. M. Richard, K. U. Lao, J. M. Herbert, *J. Chem. Phys.* **2014**, *141*, 014108.
[38] K.-Y. Liu, J. M. Herbert, *J. Chem. Phys.* **2017**, *147*, 161729.
[39] P. Jerabek, O. R. Smits, J.-M. Mewes, K. A. Peterson, P. Schwerdtfeger, *J. Phys. Chem. A* **2019**, *123*, 4201.
[40] J. M. Herbert, *J. Chem. Phys.* **2019**, *151*, 170901.
[41] I. G. Kaplan, R. Santamaria, O. Novaro, *Mol. Phys.* **1995**, *84*, 105.
[42] C. König, O. Christiansen, *J. Chem. Phys.* **2016**, *145*, 064105.
[43] D. Madsen, O. Christiansen, C. König, *Phys. Chem. Chem. Phys.* **2018**, *20*, 3445.
[44] E. E. Dahlke, D. G. Truhlar, *J. Chem. Theory Comput.* **2006**, *3*, 46.
[45] E. E. Dahlke, D. G. Truhlar, *J. Chem. Theory Comput.* **2008**, *4*, 1.
[46] P. J. Bygrave, N. L. Allan, F. R. Manby, *J. Chem. Phys.* **2012**, *137*, 164102.
[47] S. Wen, G. J. O. Beran, *J. Chem. Theory Comput.* **2011**, *7*, 3733.
[48] C. R. Jacob, J. Neugebauer, L. Jensen, L. Visscher, *Phys. Chem. Chem. Phys.* **2006**, *8*, 2349.
[49] R. Kevorkyants, X. Wang, D. M. Close, M. Pavanello, *J. Phys. Chem. B* **2013**, *117*, 13967.
[50] J. Gao, Y. Wang, *J. Chem. Phys.* **2012**, *136*, 071101.
[51] K. Kitaura, E. Ikeo, T. Asada, T. Nakano, M. Uebayasi, *Chem. Phys. Lett.* **1999**, *313*, 701.
[52] D. G. Fedorov, K. Kitaura, *J. Phys. Chem. A* **2007**, *111*, 6904.
[53] D. G. Fedorov, N. Asada, I. Nakanishi, K. Kitaura, *Acc. Chem. Res.* **2014**, *47*, 2846.
[54] S. P. Veccham, J. Lee, M. Head-Gordon, *J. Chem. Phys.* **2019**, *151*, 194101.
[55] M. E. Fornace, J. Lee, K. Miyamoto, F. R. Manby, T. F. Miller, *J. Chem. Theory Comput.* **2015**, *11*, 568.
[56] M. Svensson, S. Humbel, R. D. J. Froese, T. Matsubara, S. Sieber, K. Morokuma, *J. Phys. Chem.* **1996**, *100*, 19357.
[57] L. W. Chung, H. Hirao, X. Li, K. Morokuma, *WIREs Comput. Mol. Sci.* **2012**, *2*, 327.
[58] L. W. Chung, W. M. C. Sameera, R. Ramozzi, A. J. Page, M. Hatanaka, G. P. Petrova, T. V. Harris, X. Li, Z. Ke, F. Liu, H.-B. Li, L. Ding, K. Morokuma, *Chem. Rev.* **2015**, *115*, 5678.
[59] G. S. Tschumper, *Chem. Phys. Lett.* **2006**, *427*, 185.
[60] N. J. Mayhall, K. Raghavachari, *J. Chem. Theory Comput.* **2011**, *7*, 1336.
[61] G. J. O. Beran, *J. Chem. Phys.* **2009**, *130*, 164115.
[62] G. J. O. Beran, K. Nanda, *J. Phys. Chem. Lett.* **2010**, *1*, 3480.
[63] T. A. Wesolowski, A. Warshel, *J. Phys. Chem.* **1993**, *97*, 8050.
[64] N. Govind, Y. A. Wang, A. J. R. da Silva, E. A. Carter, *Chem. Phys. Lett.* **1998**, *295*, 129.
[65] A. S. P. Gomes, C. R. Jacob, L. Visscher, *Phys. Chem. Chem. Phys.* **2008**, *10*, 5353.
[66] A. S. P. Gomes, C. R. Jacob, F. Réal, L. Visscher, V. Vallet, *Phys. Chem. Chem. Phys.* **2013**, *15*, 15153.
[67] R. G. Parr, W. Yang, *Density-Functional Theory of Atoms and Molecules*, Oxford University Press, Oxford **1989**.
[68] E. Engel, R. M. Dreizler, *Density Functional Theory: An Advanced Course*, Springer, Heidelberg **2011**.
[69] W. Li, S. Li, Y. Jiang, *J. Phys. Chem. A* **2007**, *111*, 2193.
[70] R. M. Richard, J. M. Herbert, *J. Chem. Phys.* **2012**, *137*, 064113.
[71] R. M. Richard, K. U. Lao, J. M. Herbert, *Acc. Chem. Res.* **2014**, *47*, 2828.
[72] K. U. Lao, K.-Y. Liu, R. M. Richard, J. M. Herbert, *J. Chem. Phys.* **2016**, *144*, 164105.
[73] S. Fux, C. R. Jacob, J. Neugebauer, L. Visscher, M. Reiher, *J. Chem. Phys.* **2010**, *132*, 164101.
[74] J. P. Unsleber, J. Neugebauer, C. R. Jacob, *Phys. Chem. Chem. Phys.* **2016**, *18*, 21001.
[75] T. A. Wesolowski, H. Chermette, J. Weber, *J. Chem. Phys.* **1996**, *105*, 9182.
[76] T. A. Wesolowski, *J. Chem. Phys.* **1997**, *106*, 8516.
[77] Y. Chen, H. Li, *J. Phys. Chem. A* **2010**, *114*, 11719.
[78] G. A. Cisneros, K. T. Wikfeldt, L. Ojamäe, J. Lu, Y. Xu, H. Torabifard, A. P. Bartók, G. Csányi, V. Molinero, F. Paesani, *Chem. Rev.* **2016**, *116*, 7501.
[79] C. H. Pham, S. K. Reddy, K. Chen, C. Knight, F. Paesani, *J. Chem. Theory Comput.* **2017**, *13*, 1778.
[80] K.-Y. Liu, J. M. Herbert, *J. Chem. Theory Comput.* **2020**, *16*, 475.
[81] J. D. Bernal, R. H. Fowler, *J. Chem. Phys.* **1933**, *1*, 515.
[82] American Mineralogist Crystal Structure Database, ID 0017930, URL: http://rruff.geo.arizona.edu/AMS/amcsd.php
[83] A. D. Becke, *Phys. Rev. A* **1988**, *38*, 3098.
[84] J. P. Perdew, *Phys. Rev. B* **1986**, *33*, 8822.
[85] E. Van Lenthe, E. J. Baerends, *J. Comput. Chem.* **2003**, *24*, 1142.
[86] W. L. Jorgensen, J. Chandrasekhar, J. D. Madura, R. W. Impey, M. L. Klein, *J. Chem. Phys.* **1983**, *79*, 926.
[87] T. A. Wesolowski, J. Weber, *Chem. Phys. Lett.* **1996**, *248*, 71.
[88] H. R. Leverentz, D. G. Truhlar, *J. Chem. Theory Comput* **2009**, *5*, 1573. https://doi.org/10.1021/ct900095d
[89] J. Harris, *Phys. Rev. B* **1985**, *31*, 1770.
[90] F. W. Averill, G. S. Painter, *Phys. Rev. B* **1990**, *41*, 10344.
[91] P. Cortona, *Phys. Rev. B* **1991**, *44*, 8454.
[92] A. D. Bond, R. Boese, G. R. Desiraju, *Angew. Chem. Int. Ed.* **2007**, *46*, 618.
[93] S. Wen, G. J. O. Beran, *Cryst. Growth Des.* **2012**, *12*, 2169.
[94] A. W. Götz, S. M. Beyhan, L. Visscher, *J. Chem. Theory Comput.* **2009**, *5*, 3161.
[95] D. Schlüns, K. Klahr, C. Mück-Lichtenfeld, L. Visscher, J. Neugebauer, *Phys. Chem. Chem. Phys.* **2015**, *17*, 14323.
[96] T. Klüner, N. Govind, Y. A. Wang, E. A. Carter, *J. Chem. Phys.* **2002**, *116*, 42.
[97] J. Tölle, A. Severo Pereira, P. R. Gomes, M. Pavanello, *Int. J. Quantum Chem.* **2019**, *119*, e25801.

[98] W. Mi, A. Genova, M. Pavanello, *J. Chem. Phys.* **2018**, *148*, 184107.
[99] W. Mi, M. Pavanello, *J. Phys. Chem. Lett.* **2020**, *11*, 272.
[100] G. te Velde, F. M. Bickelhaupt, E. J. Baerends, C. Fonseca Guerra, S. J. A. van Gisbergen, J. G. Snijders, T. Ziegler, *J. Comput. Chem.* **2001**, *22*, 931.
[101] Theoretical Chemistry, Vrije Universiteit Amsterdam, ADF, Amsterdam density functional program, URL: http://www.scm.com
[102] M. Franchini, P. H. T. Philipsen, L. Visscher, *J. Comput. Chem.* **2013**, *34*, 1819.
[103] C. R. Jacob, J. Neugebauer, L. Visscher, *J. Comput. Chem.* **2008**, *29*, 1011.
[104] A. Lembarki, H. Chermette, *Phys. Rev. A* **1994**, *50*, 5328.
[105] C. R. Jacob, S. M. Beyhan, R. E. Bulo, A. S. P. Gomes, A. W. Götz, K. Kiewisch, J. Sikkema, L. Visscher, *J. Comput. Chem.* **2011**, *32*, 2328.
[106] U. Ekström, L. Visscher, R. Bast, A. J. Thorvaldsen, K. Ruud, *J. Chem. Theory Comput.* **2010**, *6*, 1971.
[107] U. Ekström et al., XCFun: Exchange-Correlation functionals with arbitrary order derivatives, **2019**, URL: https://github.com/dftlibs/xcfun
[108] D. Schlüns, M. Franchini, A. W. Götz, J. Neugebauer, C. R. Jacob, L. Visscher, *J. Comput. Chem.* **2017**, *38*, 238.

**How to cite this article:** Schmitt-Monreal D, Jacob CR. Frozen-density embedding-based many-body expansions. *Int J Quantum Chem.* 2020;e26228. https://doi.org/10.1002/qua.26228